Photon signal detection and evaluation in the adaptive optics scanning laser ophthalmoscope

Yuhua Zhang and Austin Roorda

School of Optometry, University of California, Berkeley, Berkeley, California 94720-2020, USA

To select a suitable photodetector for an adaptive optics scanning laser ophthalmoscope (AOSLO) and evaluate its performance, we characterized the signal and noise properties in the AOSLO photon detection and derived the signal-to-noise ratio (SNR). Using the SNR as the main criterion, we chose the best detector from a selection of four photomultiplier tubes (PMTs) and three avalanche photodiodes (APDs). We conducted a comprehensive evaluation of the performance of the selected detector on our AOSLO. The study presents a practical strategy that can be used to test the photodetector for either initial evaluation or subsequent performance in in-line inspection. © 2007 Optical Society of America

OCIS codes: 330.4460, 170.5810, 120.1880.

1. INTRODUCTION

In adaptive optics scanning laser ophthalmoscopy,[1] a well-selected photodetector is important for obtaining high image quality and achieving the full imaging potential of the adaptive optics scanning laser ophthalmoscope (AOSLO). The AOSLO has emerged as a promising *in vivo* real-time microscopic imaging modality for the living human eye and facilitates many applications in revealing retinal disease mechanisms and improving diagnosis.[2–4] Currently, a new-generation AOSLO is being developed toward a wider range of applications.[5] The goal of this paper is to select a suitable photodetector for the new-generation AOSLO and to evaluate the detector's performance.

The photodetector should convert the signal photons that are collected from the human retina to electrons with high quantum efficiency and low intrinsic noise in order to produce a decent video signal with a good signal-to-noise ratio (SNR). The SNR characterizes the combined effects of quantum efficiency and noise, i.e., the overall performance of a detector over a certain spectral power range of the signal light and a specific imaging system bandwidth.[6–16] Therefore, the SNR is a good criterion for deciding on a suitable detector from the selection of photomultiplier tubes (PMTs) and avalanche photodiodes (APDs), which are two types of commercially available photodetectors that may technically be used in the development of the AOSLO. Theoretically, the SNR of a photodetector may be computed from the ratio of the average signal power to the average noise power,[6] the ratio of the signal photocurrent to the noise current,[7] or the ratio of the signal photon numbers to the noise photon numbers.[8–11] Normally, the photocurrent needs be converted to voltage so that it can be processed to form a certain format of video signal. So the noise from the current–voltage conversion stage must also be taken into consideration. Webb and Hughes[9] defined a comprehensive SNR in which they considered all the contributions from different noise sources, including the statistical fluctuation of the signal photons, the dark emission, and the noise from the current–voltage amplifier. The SNR was essentially expressed as the ratio of the mean number of the signal photons received by the detector per pixel to the standard deviation of the photon fluctuation number per pixel. Their definition clearly stressed the point that the signal and noise should be counted in the imaging pixelation time and appropriately reflected the performance of a photodetector for a scanning imaging system. Thus, this definition is a good guide for choosing the photodetector. Yet the real SNR of this definition is difficult to verify experimentally from the pixelated image, as it is practically arduous to measure the signal and noise photons exactly within a certain pixelation time. The SLO imaging acquisition system, in most cases, employs a flash analog-to-digital converter (ADC) to digitize the video signal that is derived from the output of the photodetector.[12,13] When the pixelation signal triggers, a track-and-hold (T/H) circuit,[17] which is built either outside or inside the ADC architecture, first catches the instantaneous video signal within a very small part of the pixel time and holds it until the next sampling pulse comes;[13,17] then the ADC converts and transfers the data. This means that the brightness of a pixel is accounting only for the average signal level and not the exact count of the photons within the pixelation time.[12,13] The average signal level is typically conditioned by a low-pass filter, which is placed in front of the data-acquisition system. Furthermore, the pixel brightness is also affected by the video signal format and system settings. Consequently, it is hard to evaluate the real SNR with this definition. The SNR should be defined such that it is not only theoretically calculable but also cast in a way that makes it measurable with standard lab instruments in a laboratory setting. Ideally, the detector should be evaluated in a real AOSLO system, and the subsequent performance can be monitored and checked periodically while the detector is kept in an in-line setting. This is the main task of our research.

Properly characterizing the signal and noise properties is an imperative step to assessing the SNR and selecting the best detector. Compared with the conventional SLO,[18] the AOSLO has many new features. It employs a larger pupil size (eye is dilated) and scans a much smaller field of view; typically 1/10th of that of the conventional scanning ophthalmoscope. Furthermore, with AO correction for the ocular aberrations, a much smaller scanning spot is formed on the retina. Given these different conditions and also considering the laser safety standard, the AOSLO has to work with a more stringent illumination light budget, which is much lower than the power used in conventional SLOs. The SNR is always associated with a specific imaging system bandwidth. So it is important to make a reasonable estimation of the signal bandwidth so that we can correctly assess the noise properties. The detector must have the proper dynamic range to contain the signal and give good linearity.

Our study starts with a characterization of the signal and noise properties in the AOSLO photon signal detection. We assessed the signal power range according to the illumination power and further measured the signal light power from a human eye that reached the detector on our first-generation AOSLO for a range of pinhole sizes. Following the analysis made by Webb and Hughes,[9] we further studied the noise properties in the PMT and the APD and derived the SNR for these two types of photodetectors. According to the specific imaging mechanism, we made a heuristic estimation of the system bandwidth. With these studies, we were able to select the photodetector that met the criterion best from four PMTs and the three APDs that matched the light source optical spectral characteristics and had relatively high spectral responsivity. We devised a method to evaluate the real performance of the selected detector on our first AOSLO. After our new-generation AOSLO was constructed, we conducted a more comprehensive test of the detector's performance. Finally we discuss some technical issues in the selection and also the construction of the best detector for the AOSLO. The study presents a practical strategy that can be used to test the photodetector for either initial evaluation or subsequent performance in-line inspection.

2. SIGNAL AND NOISE CHARACTERIZATION

A. Signal Power Estimation and Measurement
In the AOSLO, a focused laser spot is raster scanned across the retina. Each point on the retina is exposed to a series of repeated focused laser pulses with a frequency that is equal to the frame rate of the system. The photon signal of the AOSLO is the weak reflection of the scanning beam on the retina, which is on average about 1 to 100 photons returned for every 1,000,000 photons used to illuminate the eye.[19] These photons, via the scanning optics and through a tiny pinhole that is placed at the focus point of the collection lens, reach the photodetector. Obviously, the signal power is governed by the incident light power that the scanning beam puts into the eye. However, there are limits on how much light power can be safely delivered to the retina. In the AOSLO illumination re-
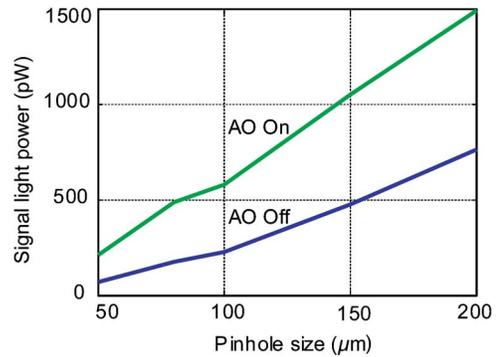

Fig. 1. (Color online) Signal light power of the AOSLO.

gime, the American National Standards Institute (ANSI Z136.1-2000) regulates that the illumination power should not exceed the maximum permissible exposure (MPE), which is computed for every known hazardous scenario.[20] In our case, we needed to consider safe levels for the following conditions: (1) MPE for a single pulse of the scanning beam, (2) MPE for the average irradiance over the entire scanned field for both thermal and photochemical hazards, and (3) MPE for multiple pulses. The MPEs are used to establish the illumination light power and thus provide a starting point for estimation of the signal light power received by the photodetector. The MPE values are specified by the light wavelength, the eye condition, and the scanning field as well as the exposure time.[21] The new-generation AOSLO will equip two laser sources whose center wavelengths are 680 and 840 nm. The frame rate is 30 Hz. The human eye is dilated during imaging, and the beam size projected on the cornea is 6 mm. The scanning field can be as small as $1° \times 1°$, which covers about $300 \times 300 \ \mu m^2$ area on the retina. We assume a 2 h continuous exposure time for each imaging session, which is a conservative overestimation. Under these conditions, the MPE for a 1 deg field for 680 and 840 nm are 2140 and 8080 μW, respectively, measured at the surface of the cornea. For a further level of safety, we use levels that are one tenth or less of the ANSI MPE, which for 680 and 840 nm are 214 and 808 μW, respectively. This extra level of safety is to account for unknown absorption or light sensitivity properties in eyes with retinal disease.

The typical levels used in our experiments range from $20 - 200 \ \mu W$ at 680 and $300 - 800 \ \mu W$ at 840 nm. Considering the losses in the optical path between the eye and the detector, the light power reaching the photodetector ranges from 0.01 to 10 nW.

Figure 1 shows the signal power reflected from a normal human eye retina and passing through a serious of pinholes of different sizes measured on the first-generation AOSLO.[1] The signals were measured with and without AO correction. The eye was dilated (one topically applied drop each of 0.5% tropicamide and 2.5% phenylephrine), and the AO correction was done over a 6 mm pupil. The laser wavelength was 660 nm, and the light power at the cornea was 75 μW. During the measurement, care was taken to ensure that ambient light did not reach the powermeter.

B. Noise in Photon Detection
Over the estimated signal power range, PMT and APD are commercially available photodetectors that may be technically employed. The noise present in these photodetectors has a significant effect on the signal photon detection.

1. Photomultiplier Tube Noise
In the AOSLO, the PMT is very well encapsulated except for a tiny confocal pinhole that is opened for receiving the signal photons. Therefore, the noise in a PMT photodetector comes from three sources[7–9,14,15]: the quantum fluctuation of the signal photocurrent, the thermionic emission of photocathode (i.e., the dark photocurrent), and the transimpedance amplifier that converts the photocurrent into voltage. The noise from the quantum fluctuation of the signal photocurrent I_P and the dark photocurrent I_D can be lumped to the shot noise in which the contribution of the signal current is dominant, while the dark current contributes little. After the internal amplification of the PMT, a minor noise characterized by the noise figure N_F, which is 1.2 in the Hamamatsu PMTs,[7] is multiplied with the total shot noise. The noise coming from the current-to-voltage conversion process is lumped to the input noise current of the operational amplifier denoted by I_A. So the total noise current I_N is

$$I_N^2 = 2eBG^2N_F(I_P + I_D) + I_A^2, \qquad (1)$$

where e is the electron charge, $e = 1.602 \times 10^{-19}$ C, B is the bandwidth of the system in hertz, and G is the internal gain of the PMT.

$$I_A^2 = i_{in}^2 B, \qquad (2)$$

where i_{in} is the input-noise current density of the transimpedance amplifier in $A/Hz^{1/2}$.

2. Avalanche Photodiode Noise
The APD has an internal photon multiplication mechanism different from that of the PMT.[6,9,14,16,22] The dark noise I_D has two contributors.[6,16,22] One is the surface leakage current I_{DS}, which flows through the interface between the PN junction and the Si oxide layer and does not flow through the avalanche region and thus is not multiplied. The other one is the internal current I_{DG}, which is generated inside the Si substrate and flows in the avalanche region, so it is multiplied with the gain factor G of the APD. So

$$I_D = I_{DS} + GI_{DG}. \qquad (3)$$

During the internal amplification, an excess noise characterized by the excess noise figure F, which is determined by the APD gain and the excess noise index of the detector's material,[6,16,22] is added to the total shot noise. The total noise current in the APD can be calculated with

$$I_N^2 = 2eBG^2F(I_P + I_{DG}) + 2eBI_{DS} + I_A^2. \qquad (4)$$

C. Signal–to–Noise Ratio
We define the SNR as the ratio of the signal amplitude to the noise amplitude. For the PMT,

$$\text{SNR} = \frac{I_P G}{\sqrt{2eBG^2N_F(I_P + I_D) + i_a^2B}}, \qquad (5)$$

while for APD,

$$\text{SNR} = \frac{I_P G}{\sqrt{2eBG^2F(I_P + I_{DG}) + 2eBI_{DS} + i_a^2B}}. \qquad (6)$$

If we set the sampling frequency equal to the Nyquist frequency of the signal, i.e., $\Delta t = 1/(2B)$, where Δt is the pixelation time, this definition of the SNR is essentially the same as the one that was defined by Webb and Hughes[9] (discussed in Appendix A).

D. Signal Bandwidth
Signal bandwidth is a very important factor in assessing the SNR of the detector as well as the related signal processing electronics design. The signal bandwidth is eventually determined by the lateral resolution of the optical system,[13] as a heuristic estimation,

$$B \approx \alpha(300/r_d)f_l/t_d, \qquad (7)$$

where α is the scanning angle in degrees; r_d is the lateral resolution of the AOSLO in micrometers; f_l is the line-scanning frequency in Hz; and t_d is the duty cycle of the line scanning, which is normally the linear region of the sinusoidal scanning path where the imaging data-acquisition system records the image. Given a line-scanning frequency of 16 kHz and a duty circle of 40%, r_d is 2.33 μm according to our previous research[23] and the bandwidths of the signal corresponding to 1°, 1.5°, and 2° scanning angles are approximately 5.0, 7.5, and 10 MHz, respectively.

3. SELECTION AND EVALUATION OF THE PHOTODETECTOR

A. Selection of the Best Detector
According to the wavelengths of the light sources that are to be employed in the AOSLO, we selected four PMTs and three APDs from the commercially available photodetectors, whose characteristics are summarized in Table 1. Basically these photodetectors have high spectral responsivity and low dark noise and thus possibly render a high SNR. Considering the fact that the rated maximum anode currents of PMT H7422-40 and H636-10 are less than 2 μA, which may significantly limit the dynamic range of the signal, we calculate only the SNRs of PMT models H7422-20 and R928 and APD models S3884, C30902E, and C30902s over the AOSLO signal power range at wavelengths 680 and 840 nm. A transimpedance amplifier C6438-01 (Hamamatsu Corporation, Japan), whose root-mean-square input-noise current density is assessed to be 45×10^{-12} $A/Hz^{1/2}$, was adopted in the computation. As can been seen in Fig. 2, the PMT H7422-20 demonstrates the best SNR and thus was selected for the new-generation AOSLO.

B. Measuring the SNR in the First-Generation AOSLO
Figure 3 shows the first AOSLO system, whose working mechanism was reported elsewhere.[1] Here we placed a

diffuse reflector at the retinal conjugate point, which was in front of the mirror M1 and prior to the scanning optics, thus generating an aligned, constant light source on the detector, which is a uniform imaging target for the AOSLO system. The light reflected from this point transits along the signal light path through the pinhole and reaches the photocathode of the PMT. We recorded the signal voltage with a digital oscilloscope 54624A (Agilent Technologies, Inc., Palo Alto, Calif.) whose sampling rate can be as high as 200 Msamples/s, and set the measuring point at the output of the amplifier C6438-01 (Hamamatsu Corporation) that is connected directly to the PMT.

We calibrated the signal power after the pinhole with careful elimination of the ambient stray light in the optical path. We also kept monitoring the image to ensure that the signal was not saturated. By measuring the mean and standard deviation of the PMT signal over one scanning line, we calculated the SNR, which is plotted in Fig. 4 with the star points. We also draw the theoretically calculated SNR for comparison. The bandwidth is limited by the amplifier C6438-01. The measured and calculated SNRs demonstrate good consistency.

C. Evaluation of the Detector in the New-Generation AOSLO

After the new AOSLO was constructed,[5] we conducted a more comprehensive test. The measurement was done over a 10 MHz bandwidth, which is limited by a low-pass filter after the amplifier C6438-01. The light wavelength was 840 nm.

Figure 5 shows the measured SNR versus the gain settings of the PMT when the target was illuminated with a constant laser power. Clearly, the SNR kept fairly stable when we increased the PMT gain; but when we increased the light power, the SNR rose to a new level.

Once we kept the PMT gain constant and increased the illumination power, the SNR improved accordingly, as shown in Fig. 6. According to the trend lines drawn from the SNR that was measured with three gain settings, the SNR is approximately proportional to the square root of the illumination power, which means that the system is photon noise limited.[9] Again, the measured SNR agrees very well with the theoretically predicated SNR, as shown in Fig. 7.

Ultimately, the photodetector's performance should be evaluated by the images taken from the human eye. We

Table 1. Characteristics of Seven Photodetectors

Detector	Spectral Range (nm)	Responsivity[c] (A/w)		Dark Current[d] (nA)	Gain	Response Time (ns)	Max. Anode Current (μA)
		at 680 nm	at 840 nm				
PMT H7422-40[a]	300–720	0.176		1.00	5.0×10^5	1.00	2.00
PMT H7422-20[a]	300–890	0.072	0.030	0.25	5.0×10^5	0.78	100
PMT R636-10[a]	185–930	0.063	0.048	2.0	4.5×10^5	2.00	1.00
PMT R928[a]	185–900	0.032	0.004	50	1.0×10^7	2.20	100
APD S3884[a]	400–1000	38	48	5.0	1.0×10^2	0.50	
APD C30902S[b]	400–1000	80	128	30	2.5×10^2	0.50	
APD C30902E[b]	400–1000	55	77	30	1.5×10^2	0.50	

[a]Made by Hamamatsu Corporation, Japan.

[b]Made by Perkin Elmer Limited, Canada.

[c]Specified at the cathode for PMT; for APD, specified at the anode with the listed gain.
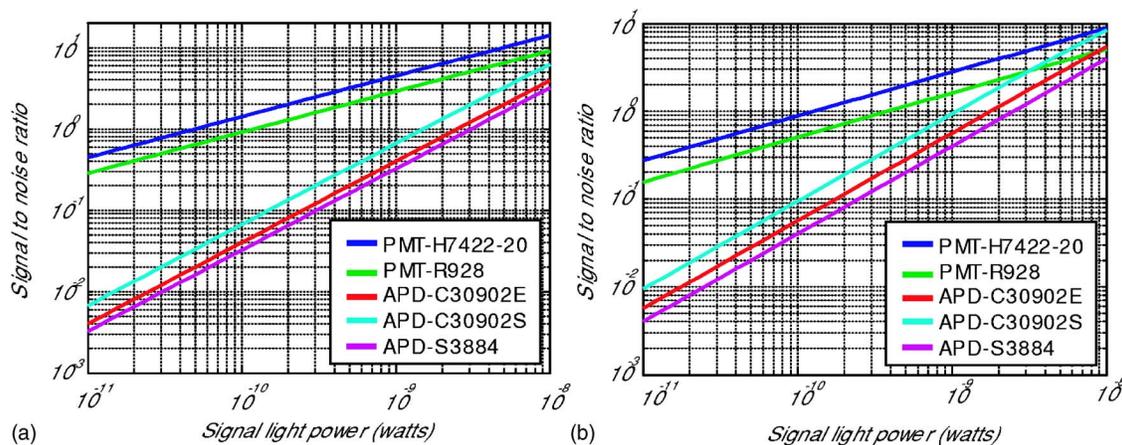
[d]Specified at the anodes with the listed gain.

Fig. 2.   (Color online) Calculated SNR of photodetectors. (a) Shows the SNRs that were calculated at 680 nm, whereas (b) plots the SNRs that were calculated at 840 nm.
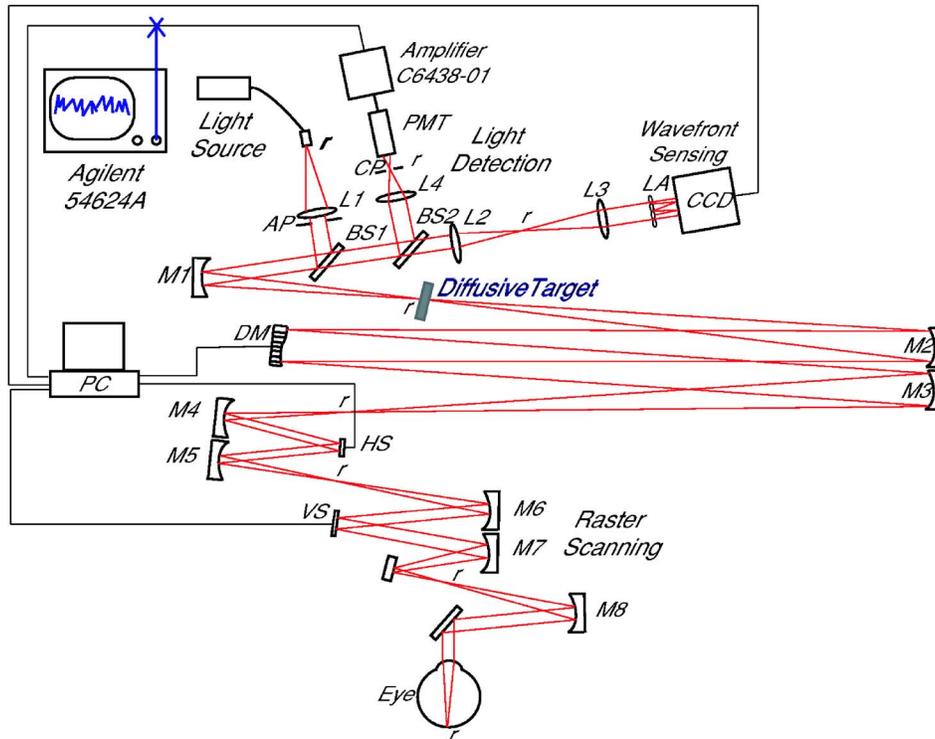
Fig. 3.   (Color online) Measurement of the SNR of the PMT. L1–L4, lenses; M1–M8, spherical mirrors; AP, artificial pupil; BS1–BS2, beam splitters; DM, deformable mirror; HS, horizontal scanner (16 kHz); VS, vertical scanner (30 Hz); LA, lenslet array; CP, confocal pinhole; PMT, photomultiplier tube. The retinal conjugate points are marked with "r."
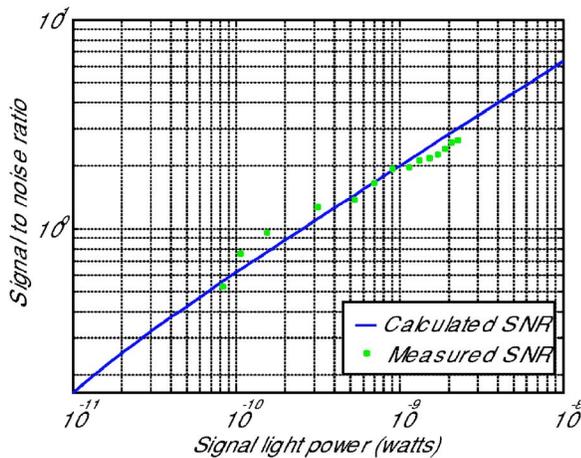

Fig. 4.   (Color online) Calculated and measured SNRs of PMT H7422-20 over a bandwidth of 50 MHz. The PMT gain was 1.2×10^5, and the laser wavelength was 660 nm.
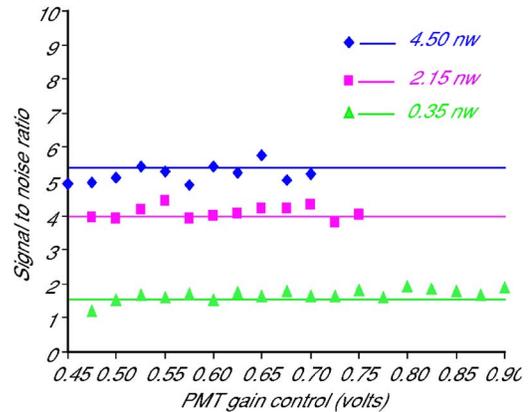
Fig. 5.   (Color online) SNR versus the PMT gain. The PMT gain is approximately $2 \times 10^6 V^{6.65}$, where V is the control voltage of the PMT. The diamonds, squares, and triangles are measured SNRs at different illumination power levels, and the solid lines are theoretical SNRs corresponding to the testing power of the light.

present two examples in Fig. 8. These images demonstrate good SNR and dynamic range.

4. DISCUSSION

In this research, we selected the PMT. However, that decision was made under the condition where we adopted a commercially available transimpedance amplifier C6438-01, which has a fairly high input-noise current density. In fact, if we calculate the SNR at the anodes of the photodetectors without taking account of the noise contribution of the transimpedance amplifier (i.e., assuming an ideal transimpedance amplifier whose input-noise current is 0),

we find that all the photodetectors present similar SNR values over this light power range (see Fig. 9). The APD modules give even better SNRs than do the PMTs. But the APD internal gain is significantly lower than that of the PMT such that when they are connected to the transimpedance amplifier, the signal is substantially deteriorated by the amplifier's input noise. In our analysis, we determined that the input-noise current density of the C6438-01 was 45 pA/Hz$^{1/2}$. We should acknowledge here that this is a very conservative estimation, since Fig. 7 shows that below 3 nW the measured SNR is greater than the theoretical prediction. If the input-noise current den-

sity is less than 5 pA/Hz$^{1/2}$, the SNR given by APD C30902S will become comparable to that of PMT H7422-20. As to APD S3884, its maximum internal gain is only 100, putting even greater demands on the noise characteristics of the amplifier.

Other PMT modules, such as H7422-40 (Hamamatsu Corporation, Japan), have higher responsivity, but their maximum output signal current at the anodes is rated at only 2 μA, which converts to a permissible illumination on the cathode of 0.011 nW. This is just at the lower end of the normal AOSLO power range. Exposures beyond this permissible level do not necessarily burn down the anode (even after long exposure times), but they can damage the GaAsP photocathode. When such damage occurs, the gain drops substantially and the output becomes very noisy,[25] which unfortunately happened to our first-generation AOLSO when we originally opted to use the H7422-40. As shown in Fig. 10, the measured SNR is significantly lower than the theoretical expectation. This photodetector is defective. For H7422-20, the maximum signal current at the anode is 100 μA and the spectral re-

(a)

(b)

Fig. 8.   (a) Single frame taken from a retinal location about 1.2° from the foveal center of a human subject with the PMT H7422-20 and the 680 nm superluminecent laser diode. The field of view of this image is 1.2° or about 360 μm on a side. The light power at the cornea was 60 μW, and the PMT gain was 2×10^5. (b) Single frame taken from roughly the same retinal location of the same subject with the 840 nm superluminecent laser diode. The image size is about 1.3° or about 390 μm on a side. The light power at the cornea was 300 μW, and the PMT gain was 2×10^5. The eye was dilated. All images have been corrected for distortions due to eye movements.[24]
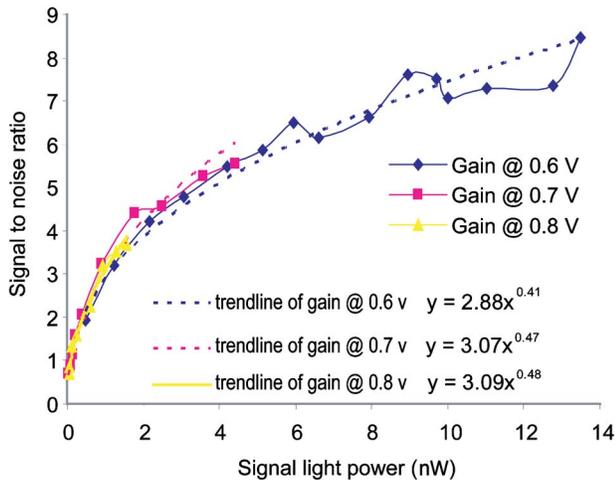

Fig. 6.   (Color online) SNR versus laser power. The PMT gain is approximately $2 \times 10^6 V^{6.65}$, where V is the control voltage of the PMT.
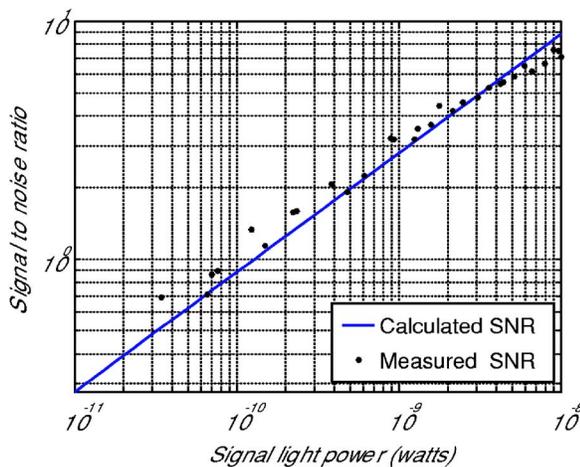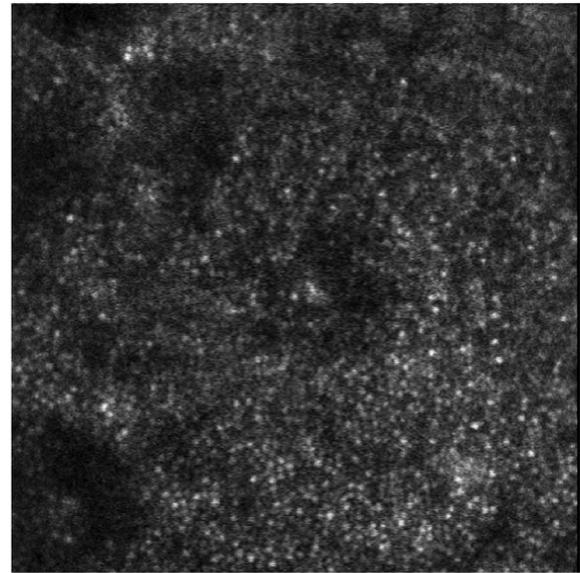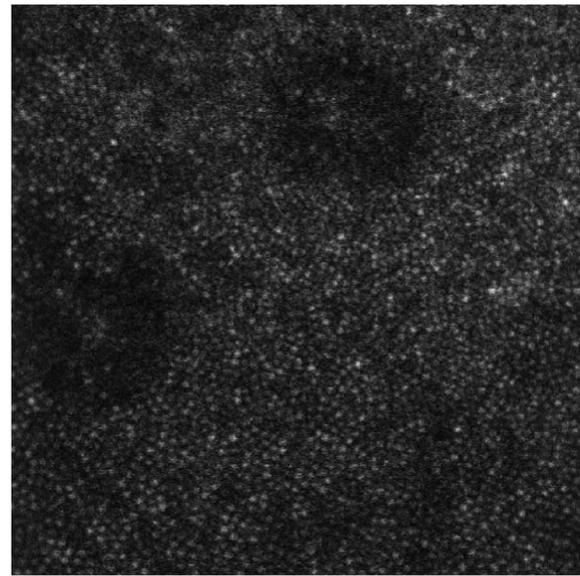

Fig. 7.   (Color online) Comparison between calculated and measured SNRs of PMT H7422-20 over a bandwidth of 10 MHz. PMT gain varies from 7.0×10^4 to 1.0×10^6. The light wavelength is 840 nm.

sponsivities at 680 and 840 nm are 0.076 and 0.030 A/W, respectively, which convert a maximum of 2.778 and 6.667 nW when the gain is set at 5×10^5 (as recommended by the manufacturer). This may explain why the measured SNRs are lower than the theoretical predicted SNRs beyond 6 nW in Fig. 7. Nevertheless, the H7422-40 PMT module is an attractive detector for imaging situations where the returning light is very low. Low-light situations include confocal imaging of the weakest scattering
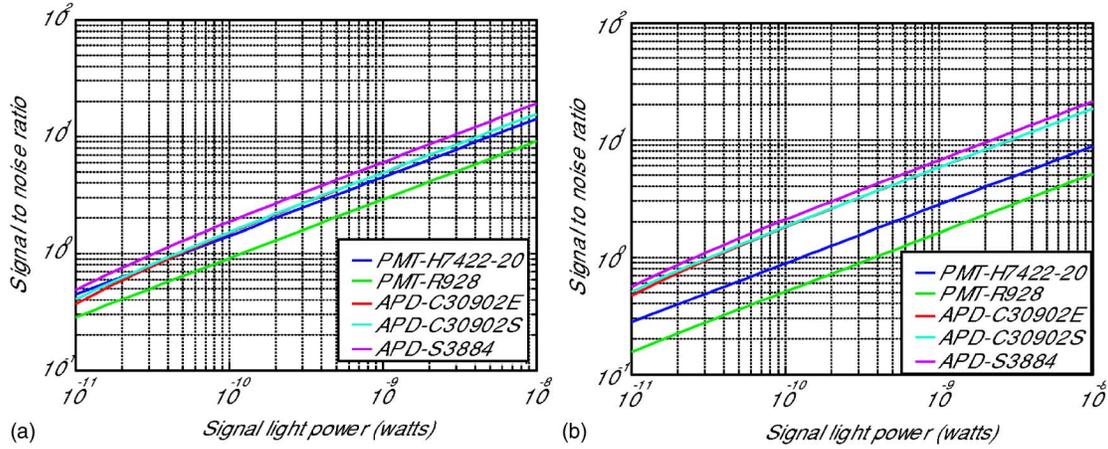
Fig. 9. (Color online) SNR of five photodetectors with an ideal transimpedance amplifier. (a) Shows the SNRs that were calculated at 680 nm, whereas (b) plots the SNRs that were calculated at 840 nm.
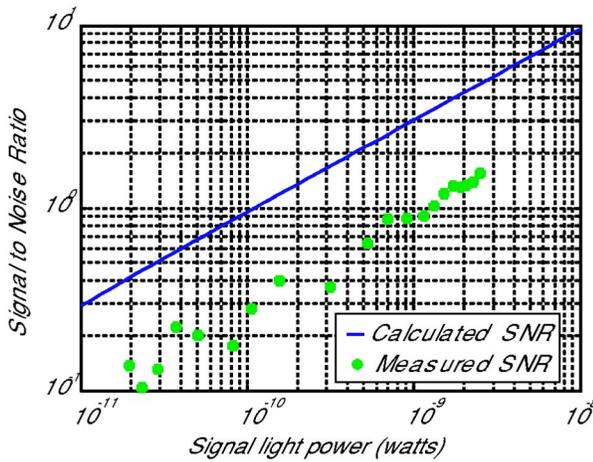

Fig. 10. (Color online) Comparison between calculated and measured SNRs of a PMT H7422-40 over a bandwidth of 50 MHz. The light wavelength is 660 nm.

layers in the inner retina, such as the ganglion cells, or autofluorescence imaging.

Over the estimated signal power and spectral ranges of the AOSLO, the PMT is more forgiving to the input noise of the transimpedance amplifier than is the APD; however, with a delicate design of a low-noise transimpedance amplifier, the APD is expected be comparable for the AOSLO photosignal detection.

5. CONCLUSIONS

The primary AOSLO detector requirements are a high SNR and a proper dynamic range. A higher internal gain photoelectron multiplication mechanism is preferable. However, the selection is very much application specific. With an appropriate analysis of the signal and noise properties, we were able to select off-the-shelf products, which are a PMT and a transimpedance amplifier, to realize photodetection and photocurrent-to-voltage conversion for the new-generation AOSLO. The real performance of the selected detector demonstrated good consistency with the theoretical expectations and is further proved in AOSLO imaging applications.[26,27]

APPENDIX A

Following Webb and Hughes,[9] suppose that the signal power is P, the quantum efficiency is η, the signal wavelength is λ, the light speed is c, the pixelation time is Δt, and the average photon number, n_P, which is counted within a pixel time at the cathode, is

$$n_p = P\eta\frac{c}{h\lambda}\Delta t. \qquad (A1)$$

In a PMT, the signal photocurrent I_P generated from the cathode is multiplied with gain G. At the anode of the PMT, the average signal photoelectron number, N_P, can be written as

$$N_P = G\frac{I_P}{e}\Delta t, \qquad (A2)$$

where e is the electron charge, whereas the noise photon number resulting from dark current I_D may be described by

$$N_D = G\frac{I_D}{e}\Delta t. \qquad (A3)$$

We lump the noise photons resulting from current-to-voltage conversion and the amplification process to get

$$N_A = \frac{I_A}{e}\Delta t = \frac{\sqrt{i_a^2 B}}{e}\Delta t. \qquad (A4)$$

We use σ_P, σ_D, and σ_A to denote the standard deviations of the photons for the signal, dark current, and amplifier noise, respectively. As the signal and dark current photons comply with the Poisson distribution, so $\sigma_P^2 = N_P$ and $\sigma_D^2 = N_D$, while $\sigma_A^2 = i_a^2 B(\Delta t)^2/e^2$. Also, considering the noise figure N_F and using Webb and Hughes' SNR definition, we have

$$\text{SNR} = \frac{N_P}{\sqrt{N_F(\sigma_P^2 + \sigma_D^2) + \sigma_A^2}}, \qquad (A5)$$

that is,

$$\text{SNR} = \frac{N_P}{\sqrt{N_F(N_P + N_D) + i_a^2 B(\Delta t)^2/e^2}}. \tag{A6}$$

Incorporating Eqs. (A2) and (A3), we get

$$\text{SNR} = \frac{I_P\sqrt{\Delta t}}{\sqrt{N_F(I_P + I_D)e + i_a^2 B(\Delta t)/G^2}}. \tag{A7}$$

In the same way, for an APD we have

$$\text{SNR} = \frac{I_P\sqrt{\Delta t}}{\sqrt{eF(I_P + I_{DG}) + eI_{DS}/G^2 + i_a^2 B(\Delta t)/G^2}}. \tag{A8}$$

From these two formulas for SNR, we can clearly find that the SNR is proportional to the square root of the pixelation time. If we set the sampling frequency equal to the Nyquist frequency of the signal, i.e., $\Delta t = 1/(2B)$, we get a good agreement between Eqs. (A7) and (5), as well as between Eqs. (A8) and (6).

ACKNOWLEDGMENTS

Corresponding author Yuhua Zhang can be reached by e-mail at yuhuazhang@berkeley.edu.

REFERENCES

1. A. Roorda, F. Romero-Borja, W. J. Donnelly III, H. Queener, T. J. Hebert, and M. C. W. Campbell, "Adaptive optics scanning laser ophthalmoscopy," Opt. Express **10**, 405–412 (2002).
2. J. A. Martin and A. Roorda, "Direct and non-invasive assessment of parafoveal capillary leukocyte velocity," Ophthalmology **112**, 2219–2224 (2005).
3. A. S. Vilupuru, N. V. Rangaswamy, L. J. Frishman, R. S. Harwerth, and A. Roorda, "Adaptive optics ophthalmoscopy for imaging of the lamina cribrosa in glaucoma," Invest. Ophthalmol. Visual Sci. **46**, E-Abstract 3515 (2005).
4. J. I. Wolfing, M. Chung, J. Carroll, A. Roorda, and D. R. Williams, "High resolution imaging of cone–rod dystrophy," Ophthalmology **113**, 1014–1019 (2006).
5. Y. Zhang, S. Poonja, and A. Roorda, "MEMS-based adaptive optics scanning laser ophthalmoscopy," Opt. Lett. **31**, 1268–1270 (2006).
6. Hamamatsu, *Characteristics and Use of Si APD (Avalanche Photodiode), Technical Information SD-28* (Hamamatsu Photonics K. K., Solid Division, 2001), pp. 5, 6.
7. Hamamatsu, *Photomultiplier Tubes—Basics and Applications*, 2nd ed. (Hamamatsu Photonics K. K., Solid Division, 1999), pp. 70–72.
8. F. Robben, "Noise in the measurement of light with photomultipliers," Appl. Opt. **10**, 776–796 (1971).
9. R. H. Webb and G. W. Hughes, "Detectors for scanning video imagers," Appl. Opt. **32**, 6227–6235 (1993).
10. R. H. Webb, "Confocal optical microscopy," Rep. Prog. Phys. **59**, 427–471 (1996).
11. C. J. R. Sheppard and D. M. Shotton, *Confocal Laser Scanning Microscopy* (Springer-Verlag, 1997).
12. J. Pawley, "Fundamental limits in confocal microscopy," in *Handbook of Biological Confocal Microscopy*, J. B. Pawley, ed. (Plenum, 1995), pp. 19–38.
13. R. H. Webb and C. K. Dorey, "The pixelated image," in *Handbook of Biological Confocal Microscopy*, J. B. Pawley, ed. (Plenum, 1990), pp. 41–51.
14. J. Art, "Photon detectors for confocal microscopy," in *Handbook of Biological Confocal Microscopy*, J. B. Pawley, ed. (Plenum, 1995), pp. 127–139.
15. J. Robert, "Photomultiplier tubes are versatile components," Biophotonics Int. **10**, 30–33 (2005).
16. Perkin Elmer, *Avalanche Photodiodes: A User's Guide* (PerkinElmer Optoelectronics Inc., 1998–2003).
17. P. Vorenkamp and J. P. M. Verdaasdonk, "Fully bipolar, 120-Msample/s 10-b track-and-hold circuit," IEEE J. Solid-State Circuits **27**, 988–992 (1992).
18. R. H. Webb, G. W. Hughes, and F. C. Delori, "Confocal scanning laser ophthalmoscope," Appl. Opt. **26**, 1492–1499 (1987).
19. F. C. Delori and K. P. Pflibsen, "Spectral reflectance of the human ocular fundus," Appl. Opt. **28**, 1061–1077 (1989).
20. ANSI, "American National Standard on the safe use of lasers," ANSI Z136.1-2000 (ANSI, 2000).
21. E. Virre, R. Johnston, H. Pryor, S. Nagata, and T. A. Furness III, "Laser safety analysis of a retinal scanning display system," J. Laser Appl. **9**, 253–260 (1990).
22. P. P. Webb, R. J. McIntyre, and J. Conradi, "Properties of avalanche photodiodes," RCA Rev. **35**, 234–278 (1974).
23. Y. Zhang and A. Roorda, "Evaluating the lateral resolution of the adaptive optics scanning laser ophthalmoscope," J. Biomed. Opt. **11**, 014002 (2006).
24. C. R. Vogel, D. Arathorn, A. Roorda, and A. Parker, "Retinal motion estimation and image dewarping in adaptive optics scanning laser ophthalmoscopy," Opt. Express **14**, 487–493 (2006).
25. G. Asencios, Hamamatsu Corporation, 360 Foothill Road, Bridgewater, N.J. 08807 (personal communication, 2003–2006).
26. J. L. Duncan, Y. Zhang, and A. Roorda, "Adaptive optics imaging of macular photoreceptors reveals differences in patients with retinitis pigmentosa and cone–rod dystrophy," Invest. Ophthalmol. Visual Sci. **47**, E-Abstract 5667/B761 (2006).
27. Y. Zhang and A. Roorda, "New generation clinically deployable adaptive optics scanning laser ophthalmoscope," Invest. Ophthalmol. Visual Sci. **47**, E-Abstract 1810 (2006).